Appl. Magn. Reson. 14, 153–167 (1998)

Applied Magnetic Resonance

Concepts in High-Frequency EPR – Applications to Bio-Inorganic Systems

E. J. Reijerse[1], P. J. van Dam[1], A. A. K. Klaassen[1], W. R. Hagen[1], P. J. M. van Bentum[2], and G. M. Smith[3]

[1] Department of Molecular Spectroscopy, University of Nijmegen, Nijmegen, The Netherlands
[2] High Field Magnet Laboratory, University of Nijmegen, Nijmegen, The Netherlands
[3] School of Physics and Astronomy, University of St. Andrews, North Haugh, St. Andrews, Scotland, UK

Received August 15, 1997

Abstract. In this contribution we describe a high-frequency high-field EPR facility which has been developed at the University of Nijmegen. We present the design of a heterodyne quasi-optical bridge based on a millimeter-wave vector network analyzer as source and detection system. The mm-waves are transported in free-space through Gaussian beam optic elements and through a corrugated guide inside the resonator insert. The Fabri-Pérot (TEM_{00n}) resonator is coupled through a metallic mesh and because of its bimodal property it can be operated using orthogonal detection leading to substantial improvement in sensitivity. In the first stage of the project, a multi-frequency CW-facility is realized covering the 100–500 GHz range. In our initial explorative experiments we demonstrate the advantages of HF-EPR of high-spin systems: Due to the large microwave quantum, transitions which would be undetectable at X-band due to the large zero-field splitting can now be observed in good sensitivity. As a model for biological high-spin systems a sample of metmyoglobin was measured at D-band (130 GHz). The $g = 5.9$ perpendicular line from the $S = 5/2$ ferric heme was detected and its line-width was compared to data previously obtained at Q-, X-, S- and L-band. As a model for biological integer spin systems the $S = 1$ signal of Ni(II) in nickel Tutton salt ($Ni(NH_4)_2(SO_4)_2$) was studied at 35 and 130 GHz.

1. Introduction

In the last decade high-frequency EPR (HF-EPR) instrumentation has been constructed in numerous groups [1–11] and probably more groups currently are in the process of developing an EPR instrument exceeding the conventional microwave frequencies of X-band (9 GHz) and Q-band (35 GHz).

Most initiatives in this field are undoubtedly driven by the increased g-tensor resolution obtainable for radical species occurring in biological systems [12, 13] and semiconductors [14]. But also the greatly increased absolute sensitivity which can be reached in single-mode resonators at 95 and 130 GHz has stimu-

lated many researchers interested in small size samples like protein single crystals [15] to enter the field of high-frequency EPR. Additional gains are obtained through the increased orientation selection in ENDOR and ESEEM [13]. These advantages prompted the development of a commercial 95 GHz EPR spectrometer by Bruker [16].

Less prominently explored is the great potential of HF-EPR in studying high electron spin species. These advantages are particularly apparent in the field of bio-inorganic chemistry. Many of the most important redox-enzymes occur in oxidation states associated with paramagnetic species featuring an integer electron spin. Usually these species are EPR silent at X- and Q-band due to a large zero field interaction. Among these are: Mn(III) in many manganese enzymes; Fe(II) in hemoglobin, oxygenase, and rubredoxins; Fe(IV) in peroxidases; Co(I) in vitamin B12 binding enzymes; Ni(II) in all Ni-enzymes; Mo(IV) in oxidases; W(IV) in dehydrogenases.

Also, for the same reason, higher doublet transitions in half-integer spin systems may be unobservable at conventional EPR frequencies, e.g., high-spin ferric iron in heme [17] and non-heme proteins [18], FeS clusters in nitrogenase, sulfite reductase, dinuclear iron oxo clusters; the Mn cluster in the oxygen evolving complex in photosynthesis.

Finally, EPR spectra may be obscured by large internal field interactions (exchange or dipolar) between clusters in a dimer. This is the case for FeS clusters in 7Fe or 8Fe ferredoxins and the Ni-Fe dimer in hydrogenase.

It will be clear that for the study of these high-spin states there is no limit to the desired magnetic field strength and microwave frequency. In order to explore the physical limits of high-frequency high-field EPR, our group is involved in a cooperation with the Nijmegen High Field Magnet Laboratory (NHFML) [19] and several European partners in a program to set up a European Large Scale Facility for HF-EPR.

In this paper we wish to elaborate on the concepts and potential possibilities of very high field/frequency EPR spectrometers as they are under construction in the Nijmegen HF-EPR facility. In addition we report on the first results obtained on high-spin systems that are relevant to biochemistry.

2. Spectrometer Design

2.1. Homodyne Setup

At 130 GHz a dedicated setup is available, based on the original homodyne design and TE_{011} cavity pioneered by the group of Lebedev [20]. The mm-wave bridge was built by the Donetsk Physico-Technical institute of the Ukrainian Academy of Sciences. In Fig. 1 the block diagram of this conventional setup is displayed. The signal from the (free running) 30 mW IMPATT source is fed into a

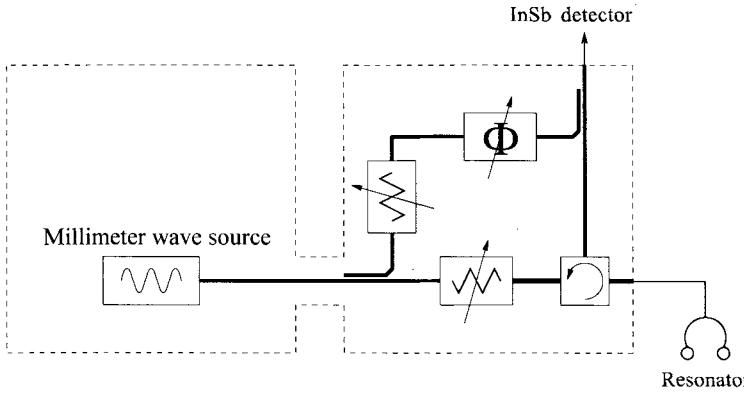

Fig. 1. Block diagram of the 130 GHz homodyne EPR bridge. Specifications: output from source: 30 mW, output from bridge: 10 mW, attenuation: 40 dB. Q of TE_{011} resonator: 1500. Sensitivity of whole system: 10^9 spins/Gauss.

standard mm-wave bridge using single mode waveguide elements. The amplitude and phase of the reference arm can be selected to enable absorption and dispersion measurements. A liquid helium cooled InSb bolometer is used as detector. An insert similar to the one described by Lebedev [20] was constructed: The mm-waves are transmitted to the TE_{011} resonator through straight oversized waveguides (WR15) and single mode (WR7) bends. At room temperature, the EPR sensitivity of this instrument was estimated using a sample of MgO with a Mn^{2+} impurity (0.003%). The absolute sensitivity was around 10^9 spins/Gauss while the concentration sensitivity amounted to 10^{11} spins/Gauss $\cdot$ cm^3. We believe that this number can still be improved since the performance of the insert is not optimal and also the electronics connected to the InSb bolometer can be upgraded.

2.2. Heterodyne Setup

In order to cover a frequency range as wide as possible, the main source/detection system of the Nijmegen HF-EPR facility is based on the principle of frequency-multiplication and sub-harmonic mixing such as is provided by the mm-wave vector network analyzer (MVNA) which has been developed by ABmm [21, 22]. The basic layout of the spectrometer is shown in Fig. 2. Two 95 GHz Gunn oscillators serve, respectively, as excitation source and detection local oscillator (LO). Both are phase locked to one of the MVNA's internal YIG oscillators which, in turn, is stabilized on an EIP source locking counter. In the excitation arm the signal of the 30 mW Gunn source is (optionally) multiplied in a Schottky diode harmonic generator (multiplication factors between 2 and 5). The circulator/resonator system is connected as "device under test" (DUT) to the vector analyzer. The signal reflected from the resonator system is mixed with the LO branch (driven by the second 95 GHz Gunn source) through a sub-harmonic mixer. The IF sig-

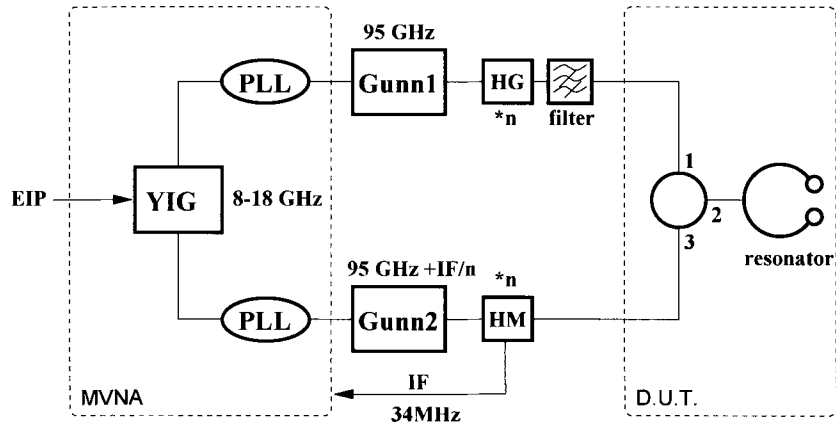

Fig. 2. General layout of the heterodyne detection scheme based on the ABmm millimeter wave vector network analyzer (MVNA).

nal is then fed into the MVNA vector detection module and subsequently digitized and stored. For each harmonic, the offset frequency between the two Gunn oscillators is selected such that after multiplication, the IF frequency is tuned to 34 MHz, i.e., the receiving frequency of the MVNA vector detector. Both amplitude and phase of the signal are stored simultaneously so that absorption and dispersion measurements are a standard feature. Also lock-in detection up to 100 kHz is provided in the basic configuration of the MVNA thus enabling field-modulation experiments. Preliminary experiments show however, that non-field-modulated heterodyne detection already provides relatively good signal to noise ratio (S/N) for many biological samples (e.g., 10 mM metmyoglobin).

In the current configuration the spectrometer is able to operate at 95, 190, 285, 380, and 475 GHz. In principle, also higher frequencies can be selected but then the available power and detector sensitivity may be insufficient for many EPR applications. External high power sources like FIR lasers and backward wave oscillators (BWO) can however, be used as reference to the MVNA oscillators thus enabling future extensions to the 500–1000 GHz range.

2.3. Gaussian Beam Optics

The multi-frequency MVNA-based system no longer employs waveguide technology for mm-wave transmission. The power losses would mount up to several dB's per meter. Instead quasi-optic techniques are used. Once mm-waves have been converted into Gaussian beams they can be transported and manipulated fairly easily with quasi-optical elements [23]. The losses in most elements are virtually negligible. In Fig. 3 the basic layout of the quasi-optical part of the setup is depicted. Most elements are mounted on a standard optical table.

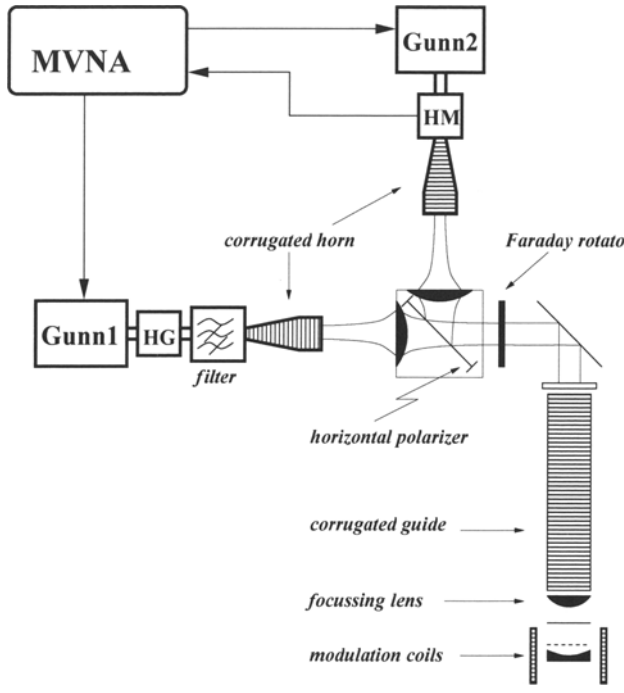

Fig. 3. Basic elements of the quasi-optical bridge. The two lenses and the polarizer are mounted on an aluminium cube shaped holder.

The multiplied excitation signal (HG) from the Gunn source, is passed through a suitable cut-off filter into a corrugated feed-horn in order to set up a fundamental Gaussian beam. Likewise, the signal reflected from the cavity is converted from a Gaussian beam into a rectangular (TE_{10}) waveguide mode and injected into the sub-harmonic mixer (HM). The theory of corrugated feed-horns is well established and design parameters can be obtained for any frequency and beam-aperture range [24]. The feed-horns in our setup have been constructed (electroformed) in the Nijmegen University workshop. The optimum frequency is centered at 190 GHz leading to a usable frequency band from 140 to 285 GHz. The beam aperture of the horns is 11 mm.

In order to refocus the mm-wave beams, suitable lenses were constructed from high density polyethylene (HDPE). Circular grooves on the lens surfaces act as $\lambda/4$ matching layers reducing reflections. Although refocusing with off-axis mirrors as it is employed by Earle and Freed [2] probably would lead to less beam-distortion and would enable complete frequency independence, we chose for lenses as they are cheap and relatively easy to manufacture for any frequency. Furthermore, they enable a very compact construction of the setup.

The combination of the wire-grid polarizer and Faraday rotator effectively acts as a circulator. The Faraday rotator is a slice of magnetized strontium hexaferrite

(Philips Ferroxdure 30) which rotates the polarization of the mm-waves passing through it. It has been demonstrated that for proper homogeneous material, the rotation of polarization is frequency independent above 100 GHz [25]. For a quasi-optical mm-wave circulator a $\pi/4$ piece is required (1.7 mm). Matching layers on both sides consist of Fluorosint. The circulator property of this combination is outlined in Fig. 4. The beam passing through port 1 has, for instance, polarization 0 and will continue unaffected through the polarizer; after passing the Faraday rotator the beam will have polarization $\pi/4$. This polarization is largely retained after the beam is reflected from the cavity. On its reverse pass through the Faraday rotator, the beam will have polarization $\pi/2$ and will thus be reflected from the polarizer through the second lens into the receiving feed-horn. The wire-grid polarizer consists of a frame with 25 μm gold coated tungsten wires with 50 μm spacing and has been constructed at St. Andrews university using a modified coil-winder [26].

The Gaussian beam is reflected from the optical table which is placed above the magnet into the insert via a flat mirror. The whole table can be moved away from the magnet to facilitate exchange of the insert and sample from the cryostat. The vacuum window of the insert is made from 3 mm HDPE. Inside the insert, the beam travels through a corrugated guide made from German silver (17 mm internal diameter). At the end of the guide, the beam is focussed on the coupling mesh of the semi-confocal Fabri-Pérot resonator by a HDPE lens. All parts of the insert are exchangeable to enable future implementation of higher frequencies. To prevent microphonic cross talk from the modulation coil to the resonator structure, the coil is mounted on a cylinder completely separated from the resonator support (i.e., the corrugated guide).

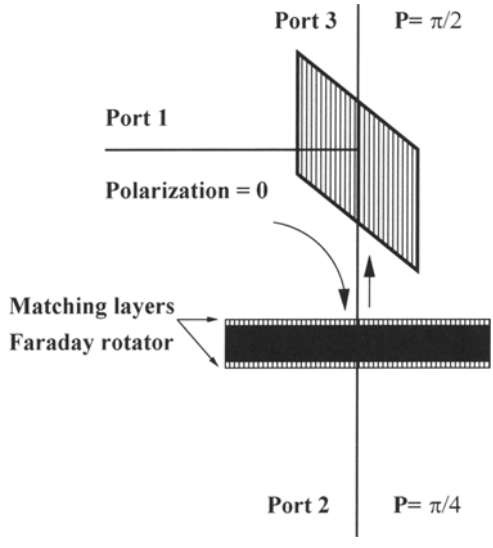

Fig. 4. Circulator as assembled from polarizer and Faraday rotator.

2.4. Bi-Modal Resonator System

The Fabri-Pérot resonator is depicted in Fig. 5. A free standing copper mesh (25 μm wires with 200 μm spacing) glued to a quartz window (0.7 mm) is used as coupling element. A thin movable dielectric sheet (PE) between the lens and the mesh is used to vary the coupling impedance of the resonator structure. The spherical mirror (also movable) is made of gold-coated quartz. The beam-waist at the mesh is about 1.5 mm leading to a spot-size of about 3 mm on the spherical mirror.

The TEM_{00n} (n = 5, 6) mode of the Fabri-Pérot resonator has interesting possibilities for bi-modal detection as is depicted in Fig. 5. Since the resonator is oversized, the sample will have little effect on the cylindrical symmetry. In this case, the resonating mode orthogonal to the mode excited by the Gaussian beam will be perfectly degenerate. The resonating mode can therefore be considered as two counter rotating circularly polarized modes. On magnetic resonance, only one of these modes is absorbed because the magnetic spins rotate according to their Larmor precession with a certain sense dictated by the sign of the Zeeman interaction. The unaffected counter rotating mode will couple net energy to the orthogonal polarization state. In other words, the magnetic resonance signal couples to both the exciting mode and the orthogonal mode and therefore causes cross-talk from one mode to the other. Since the isolation between the two polariza-

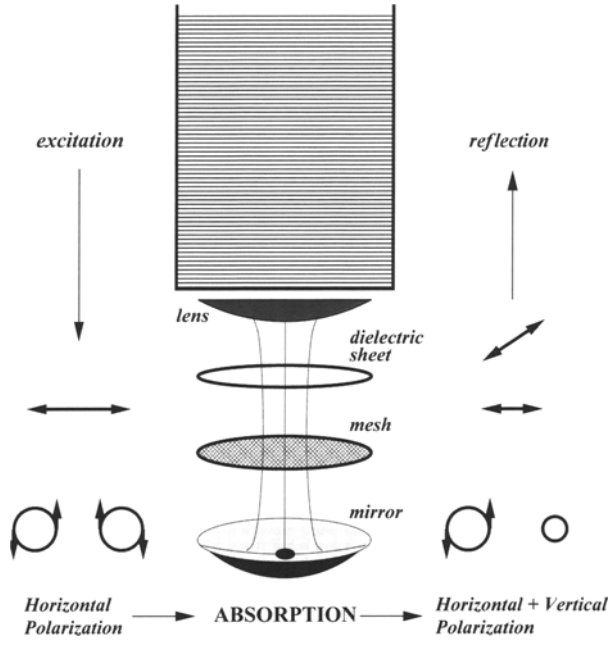

Fig. 5. Bottom part of Fabri-Pérot resonator insert illustrating the coupling elements, the spherical mirror, and the bi-modal mode of detection.

tion states can easily reach 20 dB, the orthogonal signal will be observed against a virtual "black background". The S/N ratio (when determined by source noise) will then be improved by a similar amount. By merely removing the Faraday rotator (FR), the spectrometer can be switched into the "orthogonal detection mode".

The standard way of operation is now as follows. First the resonator is tuned in the conventional direct detection mode (FR in place): the frequency is tuned by varying the Gunn oscillator bias and/or moving the spherical mirror of the FP resonator. The coupling is further optimized by adjusting the dielectric sheet. Finally the FR is removed and orthogonal detection is in operation.

The quasi-optical mm-wave system as described above has several important advantages:

- The number of optical elements is cut down to a bare minimum thus limiting problems with alignment and reducing scattering losses.
- The Faraday rotator (FR) polarizer combination is the most convenient way of separating the excitation signal from the reflected signal. The relatively high losses do not affect the spectrometer sensitivity since in the orthogonal detection mode the FR is removed.
- The orthogonal detection scheme relaxes the demands on the coupling quality of the cavity for lossy samples. Preventing the need for a double mesh coupling which could be extremely sensitive to microphonic disturbances.
- Also the effect of standing waves in the quasi optical bridge (should they occur) is effectively neutralized in the orthogonal detection scheme.

2.5. Cryostat and Magnet System

The NHFML [19] is equipped with several resistive Bitter magnets (15 and 20 T) and two hybrid magnets (25 and 30 T). The HF-EPR facility is currently built around a 60 mm bore 15 T magnet station. An Oxford CF200 He flow cryostat accommodates the resonator insert enabling operation between 4 K and room temperature. For temperatures up to 100°C a heating system has been developed. The magnet can be swept under computer control from 0–15 T in less than two minutes.

2.6. Spectrometer Sensitivity

In this section a practical and simplified analysis is given of the various noise contributions in a homodyne and heterodyne system which limit the sensitivity of the spectrometer. The system performance can be defined as the minimum detectable signal: $S_m \cdot P_e$, where S_m is the fraction of the effective power P_e reflected from the cavity in case of magnetic resonance. This amount has to be compared with all noise contributions reaching the detector leading to the following equation:

$$S_m \cdot P_e = P_D + N_A \cdot P_{LO} + P_e \cdot \Gamma_c \cdot N_A + P_e \cdot \Gamma_c \cdot F_0 \cdot N_\phi + P_e \cdot F_q \cdot N_\phi + P_e \cdot \Gamma_c \cdot N_\phi \,, \quad (1)$$

P_e is defined as the effective power reaching the detector if all power would be reflected from the cavity. P_e therefore includes all insertion and conversion losses in components and mixers. P_D is the noise floor of the detector. A typical value for a InSb bolometer is -160 dBm/Hz. The vector receiver in the MVNA has a similar noise floor. N_A represents the amplitude noise of the mm-wave source. A typical value for a Gunn oscillator at 90 GHz is around -140 dBc/Hz at 1–100 kHz offset. P_{LO} is the local oscillator power required for the detector. This number varies from -20 dBm for a Bolometer mixer to 0 dBm for a Schottky mixer. Γ_c represents the reflection of the cavity at resonance. For a critically coupled resonator values can be reached between -40 dB and -20 dB. N_ϕ represents the phase noise of the mm-wave source. F_q and F_0 represent the phase noise conversion with and without cavity; see below.

The contributions in the sum of first three terms in Eq. (1) are the most important for a homodyne detection system. It can be easily verified that for bolometric detection, they all fall below -160 dBm assuming a "standard" effective power of $P_e = 0$ dBm. The system performance parameter S_m, also interpretable as "dynamic range", is ideally in the order of 150–160 dB. Homodyne spectrometers of this type at 95 and 150 GHz utilizing a single mode TE_{011} cavity ($Q = 2000$) in absorption detection have demonstrated absolute spin detection sensitivities of $5 \cdot 10^7$ spins/Gauss and concentration sensitivities of $3 \cdot 10^{11}$ spins/Gauss $\cdot$ cm^3 thus approaching the theoretical limit [20]. We can therefore formulate an optimum (practical) limit of 150 dB dynamic range for "EPR-like sensitivity".

The remaining noise contributions (the sum of the last three terms in Eq. (1)) stem from phase noise N_ϕ of the mm-wave source. Even in homodyne systems these contributions should be taken into consideration especially when a reference arm is in operation. The conversion of phase noise to amplitude noise by a cavity and a reference arm (see Fig. 2), is given by [27]:

$$F_\phi = \sin^2(\omega_0 \Delta\tau)\left[\left(\Gamma_c(\omega) - \Gamma_c(\omega_0)\right)^2 + 4\Gamma_c(\omega)\Gamma_c(\omega_0)\sin^2(\Delta\omega\Delta\tau - \phi_c(\omega))/2\right] , \quad (2)$$

in which $\Delta\tau$ is the time delay between the excitation arm the reference arm, $\Delta\omega = |\omega_0 - \omega|$ the offset frequency from the carrier ω_0, $\Gamma_c(\omega)$ is the reflection of the cavity at frequency ω, and $\phi_c(\omega)$ the phase of the mm reflected from the cavity.

For absorption measurements the factor $\sin^2(\omega_0\Delta\tau)$ is tuned to zero by adjusting the phase in the reference arm thus eliminating, in theory, all phase noise contributions. A slight phase mismatch, however, already can introduce dispersion components into the signal carrying substantial phase noise contributions. For a matched cavity ($\Gamma_c(\omega_0) = 0$) the conversion factor (in dispersion) is given by:

$$F_q = \frac{2Q_L(\Delta\omega/\omega_0)^2}{1+2Q_L(\Delta\omega/\omega_0)^2} \quad . \tag{3}$$

For $Q_L = 2000$ and $\omega_0 = 95$ GHz, $F_q = -47$ dB at 100 kHz offset. A Gunn source locked to a YIG oscillator (as is the case for the MVNA), will produce around -90 dBc of phase noise at 100 kHz offset leading to an effective phase noise floor of -137 dBm (for $P_e = 0$ dBm). The phase adjustment should therefore bridge the gap of 23 dB requiring an accuracy of better than 4 degrees. The bi-modal detection scheme on the other hand provides an additional isolation of 20–30 dB preventing the need for phase adjustment thus making dispersion measurements possible with optimum sensitivity.

The signal directly reflected from the cavity can also cause phase noise contributions to reach the detector. Putting $\Gamma(\omega_0) = \Gamma(\omega)$ we obtain:

$$F_0 = 4\sin^2(\Delta\omega\Delta\tau)/2 \quad . \tag{4}$$

For a typical delay of $\Delta\tau = 6$ ns (equivalent to 2 meters path difference), we obtain $F_0 = -48$ dB at 100 kHz offset. In case of 20 dB cavity isolation we are left with -68 dB reduction of the phase noise (-90 dBc/Hz) reaching a safe value of -158 dBm/Hz even in dispersion.

For heterodyne detection systems the main noise contribution is formed by direct phase noise transfer to the IF signal (the last term in Eq. (1)). Unless some correlation technique is used [6, 8, 10], the phase noise is only attenuated by the cavity isolation. Taking again our example of a 95 GHz phase-locked Gunn source with -90 dBc/Hz phase noise at 100 kHz and a cavity isolation of 30 dB, we end up with -120 dB dynamic range. This leaves 30–40 dB to be gained by correlating the phase noise LO and RF branches. Obviously, the situation gets even more critical at the higher harmonics of 95 GHz.

The MVNA in its standard configuration offers a dynamic range of 120 dB when operated with 2 Gunn oscillators (95 GHz) using the 3rd harmonic (i.e., 285 GHz). Test measurements showed that this limitation is due to an equal contribution of conversion loss (in the harmonic mixer) and phase noise. In the framework of the "UMBELLA" program, the performance of the MVNA is therefore improved by implementing RF/LO correlation techniques and by using an InSb bolometer as a fundamental mixer at high frequencies (190–380 GHz) thus reducing the conversion losses considerably.

3. Preliminary Results

In this section we present preliminary results obtained with the homodyne 130 GHz setup. A central theme in HF-EPR is the wish to increase the Zeeman resolution. The possibilities to accomplish this goal vary between different spin-sys-

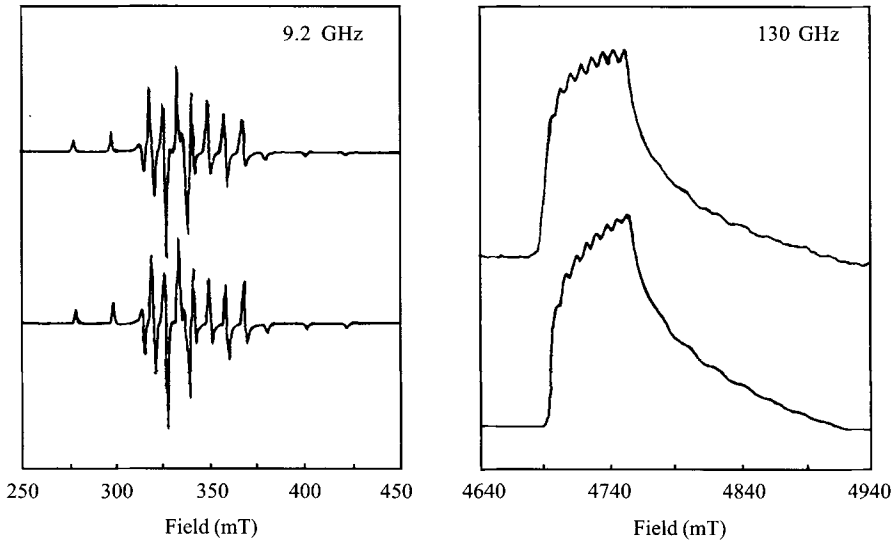

Fig. 6. Experimental (top) and simulated (bottom) spectra of aqueous VO^{2+} at 20 K. Note the complete separation of the perpendicular feature split into the eight vanadium hyperfine lines in D-band.

tems. Some Cu(II)-species already have their optimum spectral resolution at 4 GHz because at higher frequencies *g*-strain is determining the spectral line-width. For most spin systems this optimum will be found at much higher frequency but the actual optimum can only be determined experimentally.

As a pilot experiment to establish this relationship for VO^{2+} species, we studied the EPR of an acidic aqueous frozen solution of VO^{2+} at X-band and D-band (see Fig. 6). The absorption mode appearance of the D-band spectrum (130 GHz) is the result of the passage condition occurring at this frequency. It turns out that magnetically diluted $S = 1/2$ species when measured at low temperature are easily saturated by the strong B_1 field in the single mode TE011 resonator at these high frequencies. Both X- and D-band spectra were simulated with identical parameters ($g_x = 1.97$, $g_z = 1.93$, $A_x = 7.4$ mT, $A_x = 19.9$ mT) the X-band spectrum was simulated with line-width $W_x = 1.1$, $W_z = 0.8$ mT while the D-band spectrum required $W_x = 4.4$, $W_z = 5.5$ mT. From this, one can conclude that the effective *g*-tensor resolution increased about a factor of two. Apparently, at X-band the line-width is still determined by unresolved hyperfine and dipolar interactions while at D-band *g*-strain is coming partly into effect.

For high-spin systems the line-width dependence on mm-wave frequency may be much more complicated as comparted to that for $S = 1/2$ species. Distributions in *g*-parameters, HFI and the zero field parameters D and E all may affect the line-width at some point in the frequency dependence. In Fig. 7 (top) the low

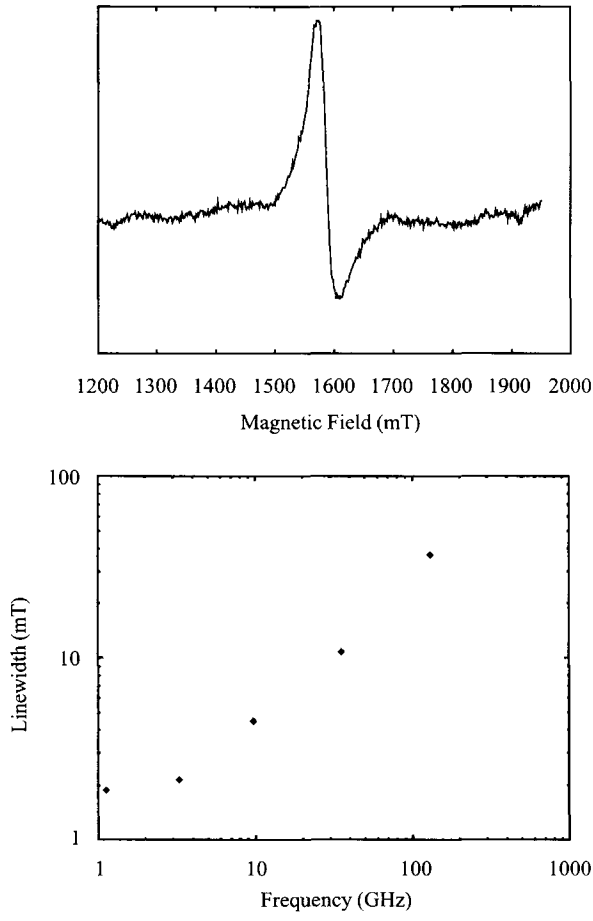

Fig. 7. Top: D-band EPR spectrum (130 GHz) of horse metmyoglobin. The $g_\perp$ feature is observed at 1587 mT (g = 5.85). Bottom: log-log plot of the line-width (mT) as peak to zero-crossing versus microwave frequency in the range 1–130 GHz.

field D-band spectrum of 10 mM horse metmyoglobin is depicted. The g = 5.9 line which is the perpendicular feature from the S = 5/2 ferric heme is characteristic for all heme proteins in the high-spin state. The line-width was measured previously at L-, S-, X- and Q-band. The frequency dependent line-width data is presented in Fig. 7 (bottom). At L- and C-band the line-width seems to be frequency independent suggesting an unresolved hyperfine mechanism. Starting from X-band, the dependence is becoming linear indicating a g-strain mechanism or a distribution in E/D.

Another reason for going to high frequency is to study integer spin systems which, in many cases, are EPR silent at conventional frequencies. As a model for Ni(II) complexes that are present in biological systems (for instance the F430

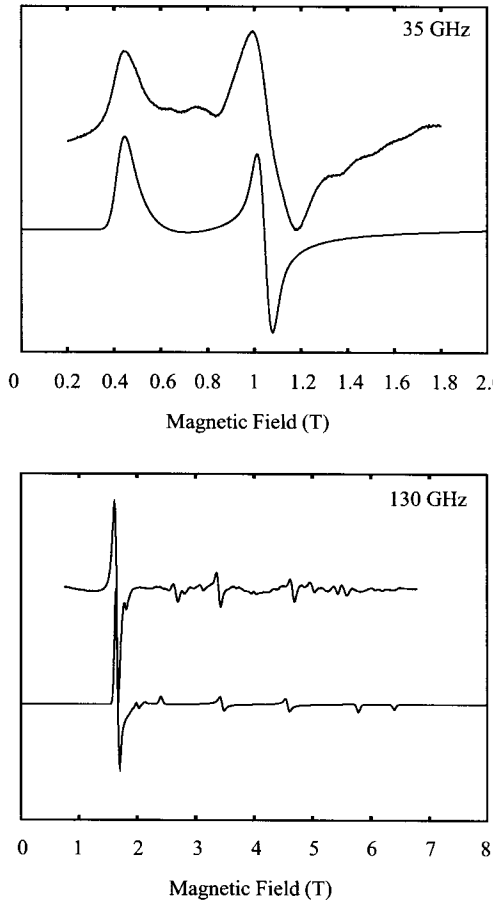

Fig. 8. The Q- and D-band spectrum of $Ni(NH_4)_2(SO_4)_2$. The lower traces are simulations with the parameters: $D = 2.24$ cm^{-1}, $E = 0.38$ cm^{-1}.

cofactor, [28]) we have studied several inorganic Ni(II) salts at Q- and D-band. In Fig. 8 the Q-band (35 GHz) and the D-band (130 GHz) EPR spectra are shown of finely powdered nickel(II) Tutton salt $Ni(NH_4)_2(SO_4)_2$. The spectra were simulated (lower traces) with EPR parameters $g_{iso} = 2.2$, $D = 2.24$ cm^{-1}, $E = 0.38$ cm^{-1} [29]. This material is completely EPR silent at X-band. At Q-band only an incomplete part of the $m = 1$ lines are visible as a broad featureless structure. Increasing the microwave frequency to 130 GHz ($h\nu = 4.3$ cm^{-1}) produces the complete triplet spectrum. The spectrum is slightly distorted due to the occurrence of microcrystals in the powder. As a consequence of the large spectral width of the $\Delta m = 1$ transitions the half field line is now the most pronounced feature. It is to be expected that for even higher zero field splittings this line will be the only well detectable feature.

4. Conclusions and Outlook

In conclusion we may state that the multi-frequency HF-EPR facility in Nijmegen offers a great potential in research possibilities both from a technological and spectroscopic point of view. The MVNA based heterodyne mm-wave bridge in combination with quasi-optical techniques offers a flexible platform for further research on optimizing spectrometer sensitivity. Most critical elements such as the reference oscillators, mm-wave sources, harmonic generators, and mixers, can be independently exchanged and optimized. The setup can be locked to external sources, to external and internal cavities. The harmonic mixers can be exchanged by cryogenic Schottky and InSb mixers. The sources and harmonic generators can be used in homodyne and heterodyne detection schemes using InSb detectors. The quasi-optical elements can be rearranged within minutes to switch from one mode of detection into another. Although the standard MVNA configuration falls short by 30 dB with respect to the ideal dynamic range of 150 dB, still very useful experiments can be performed.

The capability to switch EPR frequencies between 100 and 500 GHz opens many possibilities for the EPR spectroscopist. High-spin systems can be characterized much more thoroughly and biochemists are now able to study a range of metalloproteins at multiple frequencies in one session.

Acknowledgements

This research was supported under EEC TMR programme, grant nr. ERBFMGECT-950008 (short name: "UMBELLA"). Dr. P. Goy and Dr. M. Gross (ABmm) are gratefully acknowledged for many helpful discussions on mm-wave technology. This work was presented at the occasion of the EMARDIS-97 & Applied EPR workshop organized by Prof. N. D. Yordanov, Sofia-Bojana, June 8–17, 1997.

References

[1] Lebedev Y.: Appl. Magn. Reson. **7**, 339–362 (1994)
[2] Earle K., Tipikin D., Freed J.: Rev. Sci. Instrum. **67**, 2502–2513 (1996)
[3] Disselhorst J., Vandermeer H., Poluektov O., Schmidt J.: J. Magn. Reson. Ser. A **115**, 183–188 (1995)
[4] Brunel L.: Appl. Magn. Reson. **11**, 417–423 (1996)
[5] Burghaus O., Rohrer M., Gotzinger T., Plato M., Mobius K.: Meas. Sci. Technol. **3**, 765–774 (1992)
[6] Prisner T., Rohrer M., Mobius K.: Appl. Magn. Reson. **7**, 167–183 (1994)
[7] Wang W., Belford R., Clarkson R., Davis P., Forrer J., Nilges M., Timken M., Walczak T., Thurnauer M., Norris J., Morris A., Zhang Y.: Appl. Magn. Reson. **6**, 195–215 (1994)
[8] Prisner T., Un S., Griffin R.: Isr. J. Chem. **32**, 357–363 (1992)
[9] Becerra L., Gerfen G., Temkin R., Singel D., Griffin R.: Phys. Rev. Lett. **71**, 3561–3564 (1993)
[10] Becerra L., Gerfen G., Bellew B., Hall D.A.J.B., Inati S., Weber R., Un S., Prisner T., Mcdermott A., Fishbein K., Kreischer K., Temkin R., Griffin D.S.R.: J. Magn. Reson. Ser. A **117**, 28–40 (1995)

[11] Smith G., Lesurf J., Mitchell R., Riedi P.: IEEE Transactions on Microwave Theory and Techniques, Symposium Proceedings (IEEE MTT-S), pp. 1677–1680. Orlando 1995.
[12] Mobius K.: Appl. Magn. Reson. **9**, 389–407 (1995)
[13] Rohrer M., Plato M., Macmillan F., Grishin Y., Lubitz W., Mobius K.: J. Magn. Reson. Ser. A **116**, 59–66 (1995)
[14] Bennebroek M., Poluektov O., Zakrzewski A., Baranov P., Schmidt J.: Phys. Rev. Lett. **74**, 442–445 (1995)
[15] Coremans J., Poluektov O., Groenen E., Canters G., Nar H., Messerschmidt A.: J. Am. Chem. Soc. **116**, 3097–3101 (1994)
[16] Höfer P., Maresh G., Schmalbein D., Holczer K.: Bruker Report **142**, 15–21 (1996)
[17] Alpert Y., Couder Y., Tuchendler J., Thome H.: Biochem. Biophys. Acta **322**, 34–37 (1973)
[18] Doctor K., Gaffney B.: Appl. Magn. Reson. **11**, 425–435 (1996)
[19] Perenboom J., van Hulst K.: Physica B **155**, 74–77 (1989)
[20] Lebedev Y. in: Modern Pulsed and Continuous-Wave Electron Spin Resonance (Kevan L., Bowman M., eds), pp. 365–404. New York: John Wiley and Sons 1990.
[21] Goy P., Gross M., Raimond J. in: Proceedings 15th Conference on IR and MM Waves (Temkin R.E., ed.), SPIE Proc. **1514**, 172–173 (1990)
[22] Goy P., Raimond J., Gross M. in: Proceedings 18th Conference on IR and MM Waves (Siergrist M.R., Tran M.W., Tran T.M., eds.), SPIE Proc. **2104**, 487–488 (1991)
[23] Lesurf J. (ed.): Millemeter-Wave Optics, Sevices and Systems. London: Adam Hilger 1990.
[24] Wylde R.: IEE Proceedings **131-H(4)**, 258–262 (1984)
[25] Smith G., Unsworth C., Kang S., Franklin D., Lesurf J.: IEEE Transactions on Microwave Theory and Techniques, Symposium Proceedings (IEEE MTT-S), pp. 1665–1668. Orlando 1995.
[26] Costley A., Hursey K., Neill C., Ward J.: J. Opt. Soc. Am. **67**, 979–981 (1977)
[27] Smith G. Lesurf J.: IEEE MTT **39**, 2229–2236 (1991)
[28] Hamilton C., Scott R., Johnson M.: J. Biol. Chem. **264**, 11605–11613 (1989)
[29] Griffiths J., Owen J.: Proc. Roy. Soc. London A **213**, 459–473 (1952)

Author's address: Prof. Dr. E. J. Reijerse, Department of Molecular Spectroscopy, University of Nijmegen, Toernooiveld 1, 6525 ED Nijmegen, The Netherlands